



Ground Subsidence and Surface Cracks Evolution from Shallow-Buried Close-Distance Multi-seam Mining: A Case Study in Bulianta Coal Mine

Xuelin Yang^{1,2,3} · Guangcai Wen^{2,3} · Linchao Dai^{2,3} · Haitao Sun^{2,3} · Xuelong Li¹

Received: 17 May 2018 / Accepted: 6 December 2018 / Published online: 10 January 2019
© Springer-Verlag GmbH Austria, part of Springer Nature 2019

Abstract

To explore the law of ground deformation from shallow-buried close-distance multi-seam mining, an observation station was built in the Bulianta Coal Mine to measure and record the periodic variation of related parameters about ground subsidence and surface cracks with the advancement of working face. From the data observed from the field, it can be found that, when lower seam mining, the ground subsidence above the previously mined area was deeper and steeper than that above the left pillar; besides, the influence scope of the former was larger than that of the latter. In terms of ground cracks, the ground cracks were formed ahead of the working face and developed rapidly during the period of the breakage of the immediate roof. Besides, the average interval of the ground cracks above the previous gob was 14.75 m, and still existed and hardly changed after the advancement of the working face; while that above the left pillar was 27.8 m and most of them were closed. In addition, when the advance rate of the working face was 12.8 m/day, the advance influence distance of the mining surface crack reached the minimum of 13.6 m. This finding is helpful for protecting the surficial environment in mining area during and after mining operations and is also of significance to conduct green mining in other mining areas.

Keywords Ground deformation · Vertical subsidence · Surface cracks · Ground subsidence

Abbreviations

ϕ	Advance angle of influence
H_0	Average mining height
L_i	Advance influence distance
θ	Lagging angle of maximum subsidence velocity
l	Lagging distance of maximum subsidence velocity
W_{cm}	Maximum of ground subsidence
q	Subsidence coefficient
M	Mining height
α	Dip angle of coal seam

1 Introduction

Since the 1850s, ground subsidence induced by mining activities have become more and more serious (Feng et al. 2018; Shen et al. 2018), which is considered responsible for the perturbation of the natural ground surface, damage to public facilities, farmland, and aquifers (Can et al. 2012; Li et al. 2016; Newman et al. 2017; Tzampoglou and Loupasakis 2018). The profile, depth and influence scope of subsidence area mainly depend on the mining methods used, coal types, rock type, geological settings, geo-mechanical behaviors, and so on (Holla and Buizen 1991; Falcón et al. 1996; Zhang and Nemicik 2013; Sasaoka et al. 2015; Xia et al. 2016; Do et al. 2017).

In order to investigate the law of ground subsidence induced by underground mining, foreign and domestic scholars and engineers have conducted a great number of research work (Can et al. 2012; Park et al. 2012; Bian et al. 2014). Meanwhile, for developing subsidence theory and improving the prediction system, in recent years, a number of advanced research methods, such as the similarity simulation (Ghabraie et al. 2015; Xuan et al. 2015), numerical simulation (Zuo et al. 2009; Deck and Anirudh 2010; Liu et al. 2011; Shabanimashcool and Li 2012; Salmi et al.

✉ Guangcai Wen
wgc139@126.com

✉ Xuelong Li
lixlcumt@126.com

¹ State Key Laboratory of Coal Mine Disaster Dynamics and Control, College of Resources and Environmental Science, Chongqing University, Chongqing 400044, China

² Chongqing Research Institute of China Coal Technology and Engineering Group Corp, Chongqing 400037, China

³ National Key Laboratory of Gas Disaster Detecting, Preventing and Emergency Controlling, Chongqing 400039, China

2017), and artificial intelligence (Li et al. 2007; Hyun and Saro 2011; Shahab 2011; Torres and Rodriguez 2017), have been widely employed to analyze the mechanism of ground deformation. Besides, more sophisticated mechanism models and their corresponding calculating formulations have been set up using aforementioned methods and a body of knowledge about rock mechanics, fracture mechanics, solid mechanics, etc. (Suchowerska et al. 2016; Sepehri et al. 2017; Hamdi et al. 2018). These mechanical models and research methods are well validated in specific conditions and used to guide fieldwork.

However, the ground deformation problems caused by multi-seam mining might be more complicated, since the mechanical properties of rock strata overlying the lower coal seam would be seriously changed because of previous mining (Ding et al. 2017). Thus, the above mechanisms are not entirely applicable for ground deformation when the lower seam mining (e.g., conducting mining operations under the previous mined area). The characteristics of subsidence from sequential extraction of multi-overlapping coal seams has been studied using physical and numerical models, and the results show that the substrata movement profile, after lower seam extraction, can be separated into three different zones (i.e., virgin ground, disturbed zone, and caved zone) (Ren et al. 2014; Ghabraie et al. 2015; Suchowerska et al. 2016). Subsidence after mining from under a previously mined area is enhanced, which results from the consolidation of the ground, closure of existing cracks, and the stress release in the previous mined area (Suchowerska et al. 2013; Zhao et al. 2014; Guo et al. 2017a, b). During the process of multi-seam mining, the upper seam mining softens the overlying substrata, which makes the whole overburden rock more vulnerable to break (Ghabraie et al. 2017; Wang and Zhang 2018). Furthermore, the activation of previous gob formed by the upper seam mining may intensify the subsidence to some extent. Since the rock structure in the previous gob will become loose and have a small load-bearing capacity during lower seam mining, though it has been compressed over a long period of time after upper seam mining (Xie et al. 2014; Li et al. 2018; Zhu and Tu 2017). Consequently, the mechanical properties of rock strata play an important role for the deformation of the substrata and ground surface (Zhu 2010; Can et al. 2013; Sasaoka et al. 2015; Singh 2015; Manekar et al. 2017; Mckee et al. 2018; Hu et al. 2018; Zhang et al. 2018; Zou and Lin 2017).

Ground cracks as the other product of ground deformation not only have a great impact on the stability of surface structures, but also threaten the productivity of land and even seriously affect the safety of residents in a mining area (Li et al. 2010). Therefore, it is necessary to explore the mechanism of crack formation and development. Ground cracks caused by mining fundamentally result from that stress transmitted through rock strata from the bottom to

the surface and are also influenced by the rock properties and other characteristics of substrata. For instance, a thick layer of hard rock in the overburden could greatly reduce the mining-induced stress and slow down the dramatic surface cracks' occurrence (Wu et al. 2009; Ghosh and Sivakumar 2018). Mining methods and mining direction (including downward mining and upward mining) also affect the characteristics (such as width, depth, and shape) and the distribution of ground cracks induced by mining activities (Wu et al. 2009). The development period of ground cracks is consistent with the breaking cycle of the immediate roof. In addition, mining under a previous mined area may induce the redevelopment of the previous cracks caused by previous mining in the fracture zone. In order to clarify the formation mechanism of ground cracks, some field work has been conducted (Zhu and Lian 2012; Wang et al. 2017; Zou and Lin 2018; Wu et al. 2018). Although numerous research work related to ground subsidence and surface cracks induced by mining has been done, the research focusing on the mechanisms of ground subsidence and formation of ground cracks induced by shallow-buried close-distance multi-seam mining has been rarely reported. Thus, corresponding field work and theoretical analysis should be done to clarify the evolution law of ground subsidence and the formation mechanism of ground cracks in under such geological conditions.

2 Research Objectives

In terms of ground subsidence and cracks caused by underground mining, many experts have conducted a number of field measurements (Hu et al. 2014; Guo et al. 2017a, b; Qian and Fang 2018) and investigated the related law and mechanisms (Ju and Xu 2015; Lu et al. 2017; Zhou et al. 2017). Considering current theoretical defects and technique requirements from field operations, the principal objectives of this research are as follows:

1. Obtaining the basic features of ground subsidence induced by shallow-buried close-distance multi-seam mining;
2. Analyzing the dynamic process of ground subsidence and calculating the related parameters;
3. Exploring the evolution law of ground subsidence by comparing the features of ground subsidence because of mining under the overlying goaf zone and overlying pillars zone based on the field data;
4. Acquiring the basic shape features, distribution characteristics and evolution law of ground cracks;
5. Investigating the formation mechanics and making reasonable prediction for the development of ground cracks caused by multi-seam mining.

3 Research Area and Field Monitoring Methods

3.1 Basic Information of Bulianta Coal Mine

Bulianta Colliery is located in the southeast of the Inner Mongolia Autonomous Region, belongs to the Bulianta Township (Fig. 1). It is the biggest modern underground coal mine in the world (Fan and Zhou 2010), which was constructed by the Shendong Coal Corporation. The main geological characteristics of the mining area include thick coal seams, shallow buried depth and thick loose soil layers. Currently, the mine is extracting 2-2 coal seam as the extraction of 1-2 coal seam at the upper panel has been finished by room and pillar mining method 3 years ago.

However, because of geological conditions and mining methods, large numbers of coal pillars were left during the 1-2 coal seam mining period. During the observation period, many special phenomena of ground deformation occurred with the extraction of 2-2 coal seam, which is obviously different from the extraction of 1-2 coal seam. Some infrastructure was seriously damaged (Fig. 2), which directly influence the life of local residents.

The working coal seam at panel 22307 (Fig. 1b) is 2-2 coal seam, which is typically shallow with average depth of 100 m. It has an average thickness of 7.25 m ranging from 6.8 to 7.7 m, an average dip angle of 3° ranging from 1° to 3°. The tendency retreat longwall mining method was employed for a mining height of 6.8 m. The width (toward direction) and length (e.g., advancing direction) of working face are 300 m, 4954 m, respectively. Besides, thick soil

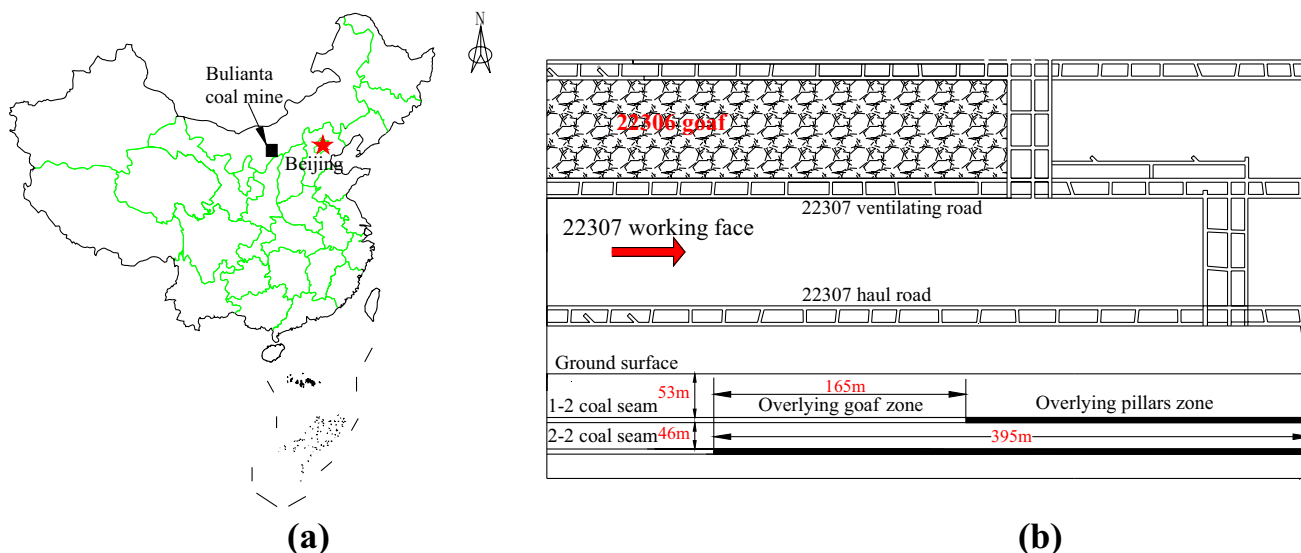


Fig. 1 Study site. a Location of Bulianta coal mine in China; b roadway layout of 22307 working face and positional relationship between 1# and 2# coal seams



Fig. 2 Damage to buildings and roads in mining areas

layers with thickness of 8–23 m mostly cover the whole panel. Table 1 lists the simplified geological settings of the working panel.

3.2 Field Monitoring Methods

3.2.1 Ground Subsidence Monitoring Method

The observation station was set on the ground surface covering the working face 22307. It included three observation lines, e.g., a tendency observation line (named line Q) along the working face direction, two toward observation lines (named line Z and line C) perpendicular to the working face direction. The tendency line was set on the surface corresponding to the central line of the working face, partially located above the previous gob and partially located above the left pillar with a critical point of Q12. Besides, it contained 27 observation points named Q1–Q27, with a fixed interval of 15 m and a total length of 395 m. Moreover, Q1 was set as the control point of line Q. Line Z, one of the toward observation lines, above the previous gob, contained 31 observation points named Z1–Z31, with a fixed interval of 30 m and a total length of 900 m. Meanwhile, Line C, above the left pillar zone, had the same arrangement as Line C. In addition, Q1, Z1, and C1 were separately set as fixed points (e.g., control points) in their lines (Fig. 3).

Generally, the observation points should be set up on the ground surface within the influence scope caused by mining. Meanwhile, the following rules should be obeyed:

1. Observation points should be located on the main section of the ground subsidence basin if possible.
2. The length of the observation lines should sufficiently cover the whole influence scope of the ground subsidence basin.
3. Observation points should be set with proper distances from each other and not be affected by the adjacent working face according to the field conditions and the research purpose.
4. Control points should be set at the both ends of the observation lines. Generally, they are set outside the influence scope of the ground subsidence basin. If there is a frozen soil area, they should be laid below the frozen soil layer 0.5 m to guarantee their stability.

3.2.2 Ground Cracks Monitoring Method

Underground activities will not only cause surface subsidence, but also ground cracks, which directly or indirectly influence the human activities and even damage the ground structures (Zhou et al. 2017). Thus, it is significant to investigate the formation mechanics and the development law of

Table 1 Simplified geological settings in panel 22307

Lithology	Depth (m)	Height (m)	Density (kg/m ³)	Compressive strength (MPa)	Elastic moduli (GPa)
Aeolian sand	6.42	6.42	–	–	–
Coarse sandstone	12	5.58	–	–	–
Sandy mudstone	15.5	3.5	2064	17.10	1.68
Mudstone	17.92	2.42	2376	40.22	3.37
Sandy mudstone	20.3	2.38	2495	23.68	3.31
Medium-grained sandstone	21.36	1.06	2178	–	–
Sandy mudstone	24.35	2.99	2342	29.02	3.60
Fine-grained sandstone	25.2	0.85	2295	36.65	6.95
Sandy mudstone	27.34	2.14	2425	48.63	7.27
Mudstone	29.7	2.36	2456	55.7	6.37
Sandy mudstone	33.63	3.93	2409	53.39	7.01
1-1 coal seam	34.75	1.12	1522	–	–
Medium-grained sandstone	45.9	11.15	2480	32.83	7.15
Sandy mudstone	46.9	1	2347	–	–
Medium-grained sandstone	47.87	0.97	2554	49.34	9.24
1-2 coal seam	53.39	5.52	1273	22.33	1.76
Sandy mudstone	57.36	3.97	2359	30.58	5.19
Fine-grained sandstone	60.26	2.9	2401	47.97	6.36
Medium-grained sandstone	90.14	29.88	2343	39.34	8.22
Sandy mudstone	91.9	1.76	2379	45.66	6.60
2-2 coal seam	99.37	7.47	1274	20.94	2.04

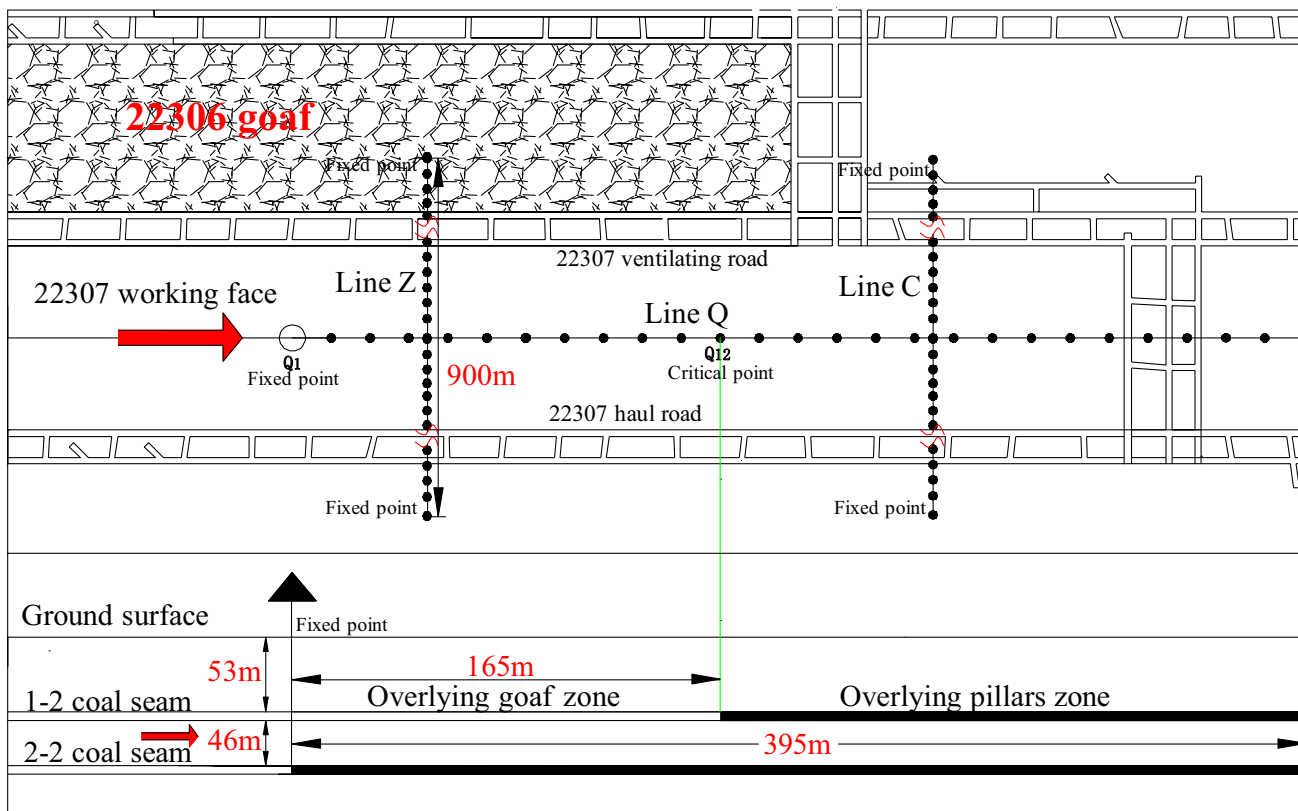


Fig. 3 22307 working arrangement of measuring points

mining-induced ground cracks and further put forward corresponding protective measures. In this paper, in order to obtain the distribution situation of surface cracks along the working face, related observations were conducted for several times, including measuring and recording the position, width and length of the cracks. Meanwhile, the temporal and spatial variation characteristics of typical cracks should be recorded to explore the relationship of cracks development versus the mining activities. In addition, considering that the cracks development may be closely related to the movement of overlying strata, related data which can reflect the overlying strata movement should be recorded.

3.3 Measurement Work

After establishing the observation stations, the measurement work of ground subsidence and cracks should be periodically and simultaneously conducted during the recovery of working face 22307. It mainly consisted of measuring and recording the height variation of observation points, the width variation and positions of ground cracks, the profile and the distribution of ground cracks. During the observation period, a Topcon DL-501 electronic level and an M-500 GNSS receiver were employed to measure the ground deformation. In addition, the measurement work continued until

that the ground deformation was stable. Figure 4 shows the daily measurement work in the stopping duration.

4 Monitoring Results and Analysis

4.1 Characteristics of Ground Subsidence Basin After Multi-seam Mining

4.1.1 Subsidence Characteristics of Tendency Measurement Line

The final subsidence of line Q (see Fig. 3) is plotted in Fig. 5, which reflects the characteristics of tendency section of the ground subsidence basin. From Fig. 5, we can see that the maximum value of ground subsidence above the previous gob was 5847 mm and occurred at the point Q8 with a distance of 105 m from the fixed point (Q1). While the maximum value of ground subsidence above the pillar zone, occurred at the Q12 with a distance of 165 m from the fixed point (Q1) was 3638 mm. Overall, the ground subsidence above the previous gob was deeper and steeper than that above the pillar zone. This phenomenon may result from the significant reduction of bearing capacity of the overlying

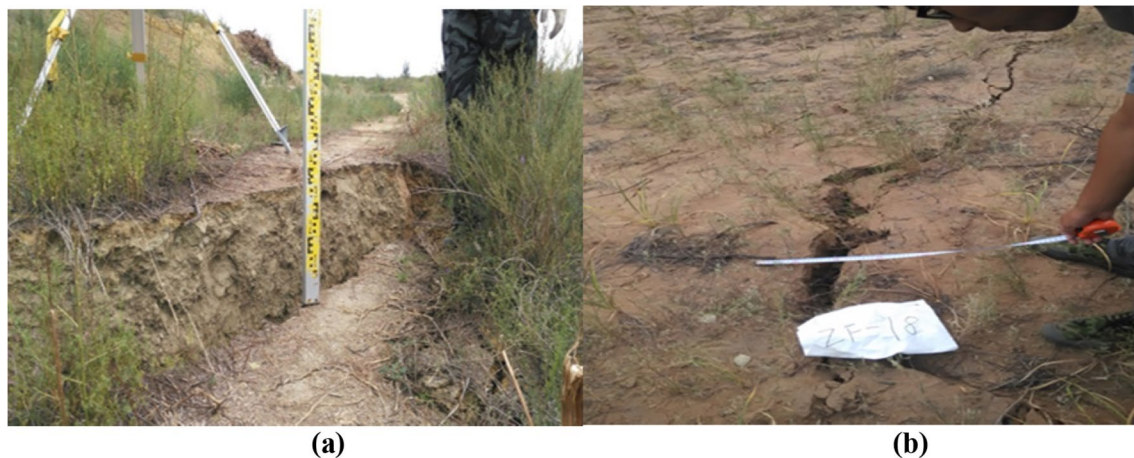


Fig. 4 Daily measurement work. **a** Height measurement for observation points; **b** width measurements for ground fissures

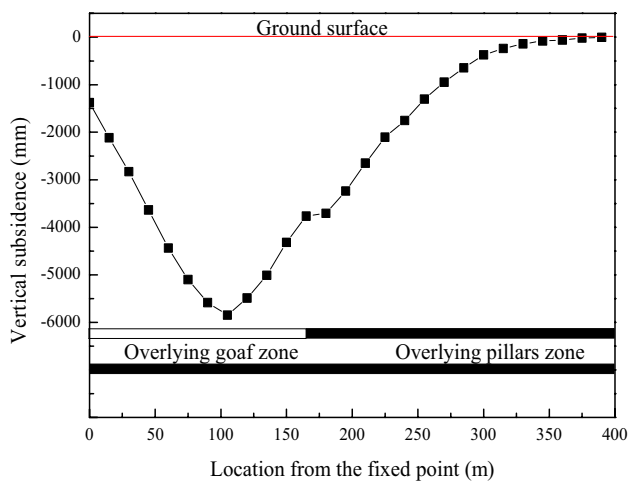


Fig. 5 Subsidence curve of line Q

strata in the previous gob induced by lower seam mining together with the effect of its own weight.

Figure 6a shows the tilt value of the observation points in line Q, which describes the features and severity of ground subsidence. The maximum tilt value of the ground above the previous gob was 53.6 mm/m at Q5, while the maximum tilt value of the ground above the pillar zone was 46.1 mm/m (absolute value) at Q11. Besides, we can see that tilt value of the ground above the previous gob was at a higher level. Meanwhile, the tilt value was the larger at the center of the tilt curve and decreased from the center to the brim. This reflects that the ground subsidence was the result of transmission of strata deformation induced by mining activities from bottom to the top.

The curvature of the observation points in line Q is presented in Fig. 6b, which reveals the unevenness of the ground surface. The maximum curvature value of the ground above

the previous gob was 3.2 mm/m² at Q2, and then there was a dramatic decrease at Q3. While, the maximum curvature value of the ground above the pillar zone was 2.2 mm/m² at Q13. In addition, from Q9 to Q23, the curvature variation was a severe oscillations type, which means that the ground surface deformation in this region was more complicated.

4.1.2 Subsidence Characteristics of Toward Measurement Line

Figure 7 presents the final profiles of line Z and line C (see Fig. 3). The maximum subsidence values of lines Z and C are 4381 mm, 2688 mm, respectively, and they were all located in the middle of the working face. Besides, the two curves were approximately symmetric about the center of the working face. However, the average subsidence of line Z was much bigger than line C. This phenomenon may have been caused by the activation of the previous gob, e.g., the overlying strata in the previous gob broken again because of lower seam mining, which resulted in the intensification of ground subsidence. Moreover, the affected scope of ground subsidence was bigger than the width of the working face (between the haul road and the ventilating road), which indicates the mining activities not only caused the vertical subsidence, but also induced the horizontal deformation of the rock strata and ground surface.

Figure 8a demonstrates the tilt variation of lines Z and C, which reflects the change of subsidence value in unit distance. The maximum tilt values of lines Z and C were 21.6 mm/m and 16 mm/m, respectively, at a distance of 60 m from the haul road. Furthermore, the curves tilt value in the scope between the haul road and ventilating road was higher than outside in term of absolute value, which reveals that the ground in the affected scope of mining activities subsided to a greater extent. In addition, the tilt value of line Z was obviously higher than

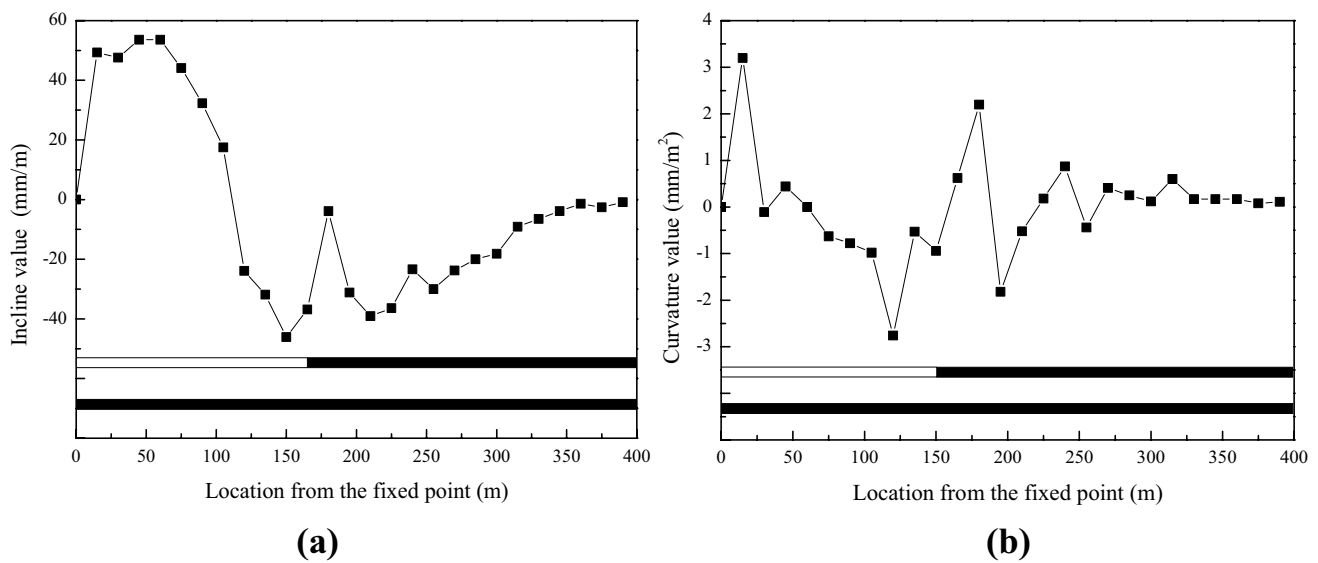


Fig. 6 a Tilt curve of line Q; b curvature of line Q

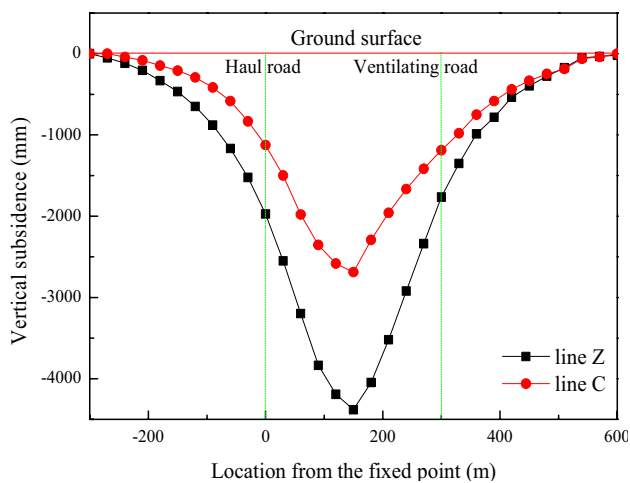


Fig. 7 Toward sinking curves of lines Z and C

line C in terms of absolute value, which reflects that the profile of line Z is steeper than line C.

The curvature variation of lines Z and C is illustrated in Fig. 8b. The maximum curvature values of lines Z and C were 0.7 mm/m^2 (absolute value) and 0.6 mm/m^2 , respectively, which separately corresponded to the points of maximum subsidence of the ground surface. The curvature values in the middle part of the working face (between the haul road and the ventilating road) were bigger.

4.2 Dynamic Variation of Ground subsidence Induced by Multi-seam Mining

Figure 9 demonstrates the process of ground subsidence with the working face proceeding. The subsidence gradually increased with the advancement of the working face, together with the enlargement of the deformation scope of ground. At the same time, the location of maximum subsidence of ground moved forward with the advancement of the working face (highlighted with broken black lines). When the working face advanced 220 m from the fixed point, the maximum subsidence reached 3948 at point Q8. Thereafter, the location of maximum subsidence of ground never changed with the advancement of the working face; however, the subsidence still continually increased until it reached 5847 mm with the working face approaching 450 m from the fixed point. Apparently, it occurred at the ground above the previous gob. For the subsidence above the left pillar, the maximum value was 3638 mm at point Q13. The subsidence velocity of the ground above previous gob was bigger than the part above left pillar.

Figure 10a reflects the tilt variation of the ground surface with the advancement of the working face. The distribution of the tilt value along the observation line hardly changed with the advancement of the working face, but the tilt value of each point increased at various degrees with the advancing of the working face.

As can be seen from Fig. 10b, in the early stage of mining, the curvature of the surface was relatively small. However, with the advancement of the working face, the curvature of each point gradually increased. When the working face approached 320 m from the fixed point, it never changed.

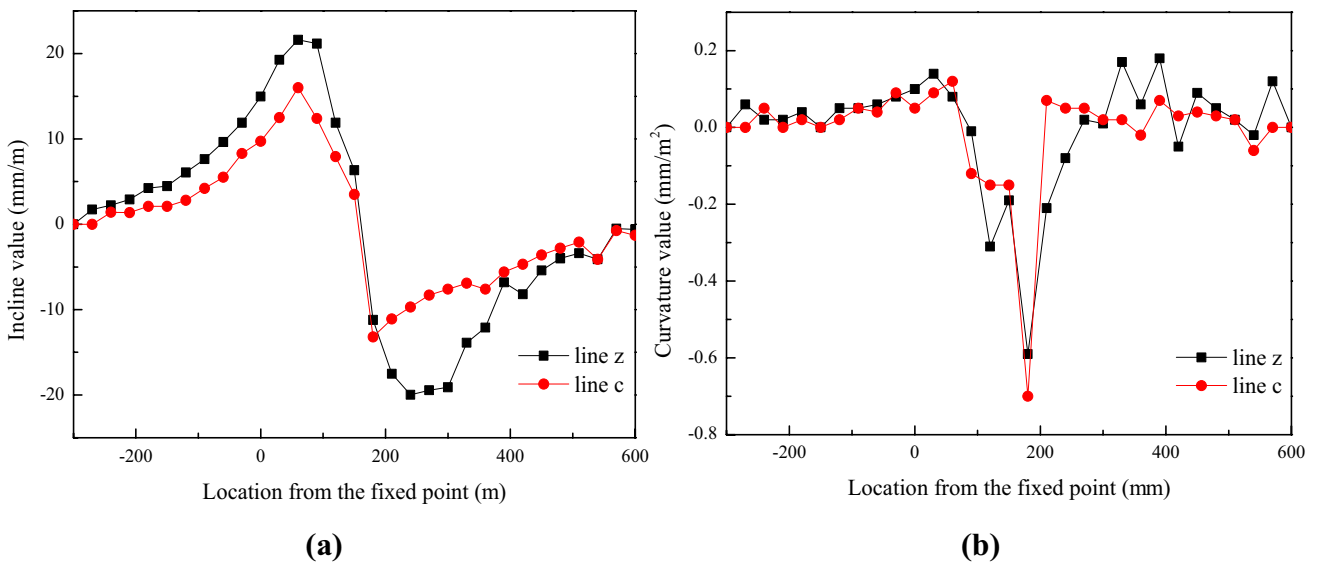


Fig. 8 Toward a tilt curves; b curvatures of lines Z and C

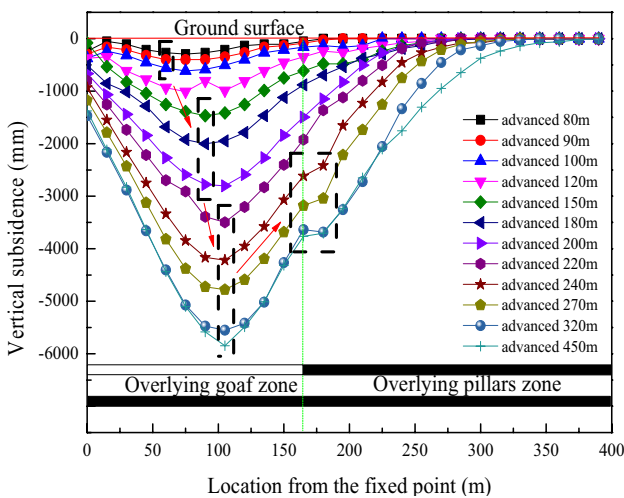


Fig. 9 Tendency sinking curves with advancement of the working face

4.3 Comparison of Related Parameters About Subsidence

4.3.1 Advance Angle of Subsidence Influence

Generally, ground subsidence occurs beforehand with the advancement of the working face because of mining activities. In the condition of full mining or nearly full mining, the advance angle of subsidence influence is the angle between the line that connects the point of 10 mm subsidence on the main section of the ground subsidence basin and the position of the working face, and the horizontal line on the side of the pillar. As can be seen from Fig. 11, ω_1 is the ground

subsidence curve corresponding to the working face reaching A, on which the subsidence value of point 1 is 10 mm, and ϕ is the advance angle of influence when the working face reaches A. The advance angle of influence is an important parameter, which is mainly used to judge the scope affected by mining activities. It can be calculated as follows:

$$\phi = \arctan \frac{H_0}{L}, \tag{1}$$

where H_0 is the average mining depth; L is the advance influence distance (see Fig. 11).

Based on the recorded advance influence distances observed in different periods with the advancement of the working face, the advance angle of influence can be obtained by combining with Eq. 1. Thus, through calculation, the advance angle of influence above the previous gob is 44.52° , together with the advance influence distance of 101.70 m; and the advance angle of influence above the pillar zone is 56.84° , together with the advance influence distance of 65.33 m.

4.3.2 Lagging Angle of Maximum Subsidence Velocity

The lagging angle of maximum subsidence velocity is the angle between the line, connecting the point with maximum subsidence velocity on the main section of the ground subsidence basin and the position of working face, and the horizontal line on the side of the gob. For instance, V_{AB} is the subsidence velocity curve corresponding to the working face reaching B (see Fig. 12), on which the subsidence velocity of point a is maximum, and then ϕ_1 is the lagging

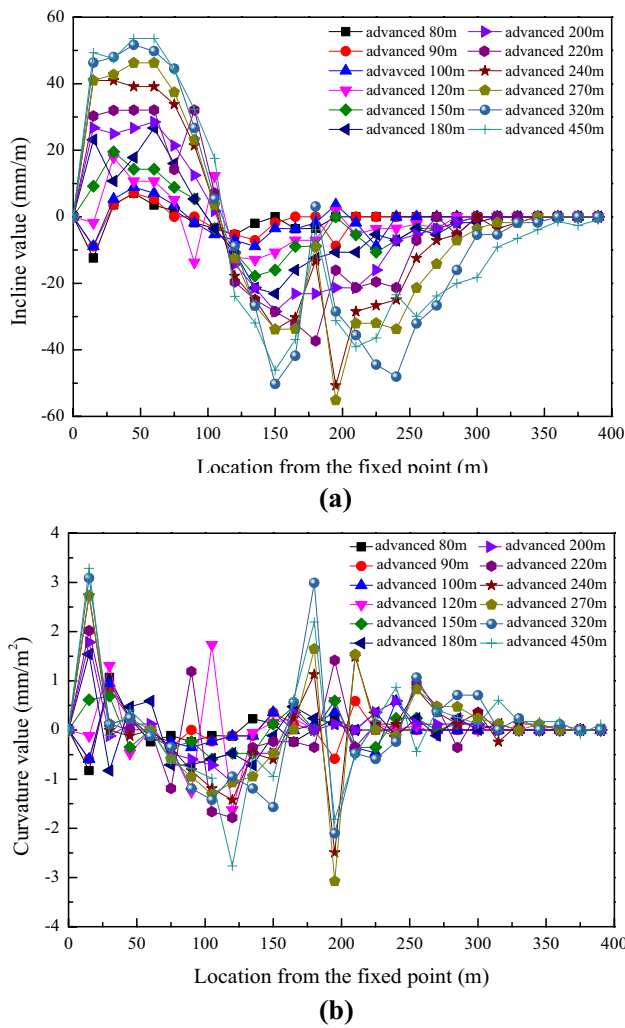
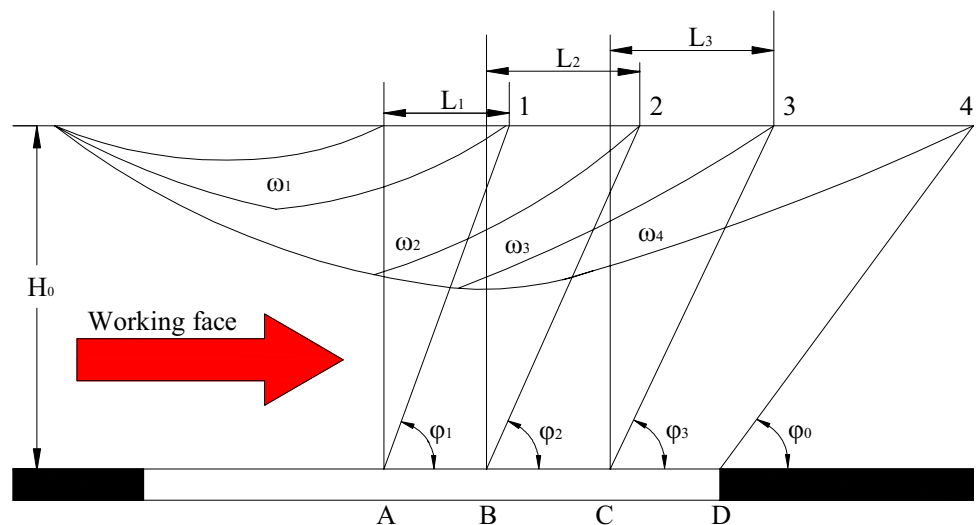


Fig. 10 a Tilt curves of tendency line with the advancement of the working face; b curvature curves of tendency line with advancement of the working face

Fig. 11 Schematic diagram of advance angle of influence



angle of maximum subsidence velocity when the working face reaches a. Therefore, it can be defined as follows:

$$\theta = \arctan \frac{H_0}{l}, \tag{2}$$

where H_0 is average mining depth, m ; l is lagging distance of maximum subsidence velocity (Fig. 12), m . Through calculation, the lagging angle of maximum subsidence velocity above the previous gob is 54.46° , while that above the pillar zone is 41.99° .

4.3.3 Subsidence Coefficient

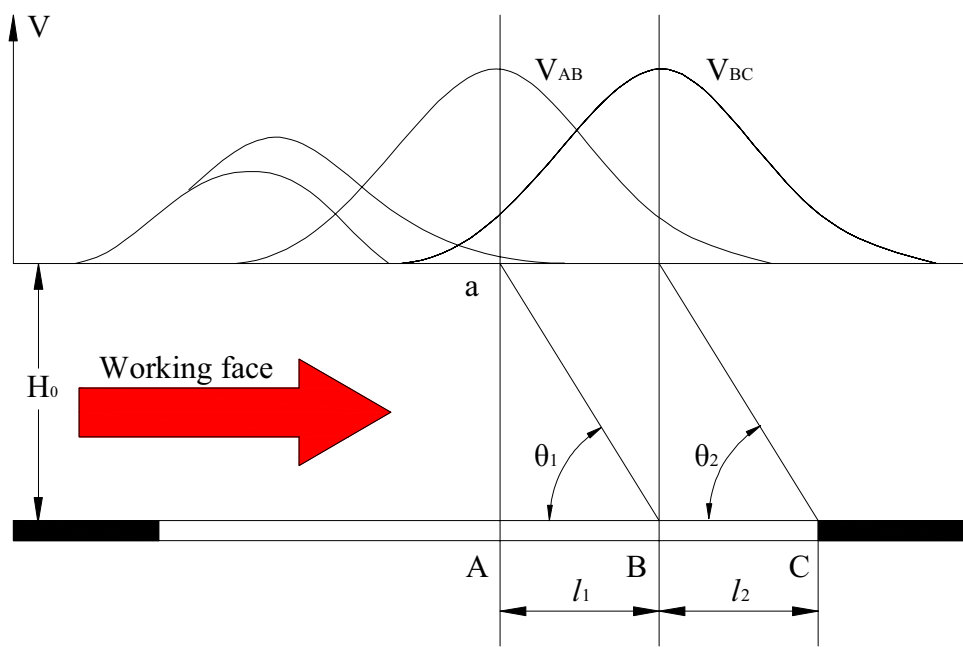
The subsidence coefficient reflects the relationship between the maximum of ground subsidence and mining height under the circumstance of full mining. Generally, it is stable in the same mining condition (full mining or non-full mining). The subsidence coefficient is calculated using Eq. 3 in the condition of full mining or super-full mining (Xu 2015).

$$W_{cm} = qM \cos \alpha, \tag{3}$$

where W_{cm} stands for the maximum of ground subsidence; M stands for the mining height; α stands for the dip angle of coal seam; and q stands for the subsidence coefficient.

Generally, the subsidence coefficient, q , is closely related to the property of immediately overlying strata, mining methods, and methods of controlling the roof. For instance, if the overlying strata are hard, the surface subsidence coefficient is small and vice versa. Based on the field data obtained, the working face 22307 was fully exploited, and the maximum ground subsidence above previous gob and that above left pillar are 5847 mm and 3638 mm, respectively; mining height is 6.8 m; tendency of coal seam is 3° . Therefore, the subsidence coefficient of ground above previous gob is 0.85, while that above the pillar zone is 0.53.

Fig. 12 Angle of maximum subsidence velocity schematic diagram. **a** Temporary cracks, **b** permanent cracks



Parameters related to surface deformation caused by multi-mining under different strata are listed in Table 2. Ground subsidence above the previous gob is much greater than that above the left pillar. Furthermore, the advance angle of influence and the lagging angle of maximum subsidence velocity, caused by ground subsidence, above the previous gob are also bigger than that above the pillar zone, which indicates that mining under the conditions of the previous gob induces a wider range of ground deformation. The subsidence coefficient of the ground above the previous gob was greater. This may be due to that the immediately overlying strata above the previous gob have undergone the process of caving–fracturing–separation–deformation from upper seam mining, which destroyed the original state of the overlying strata and decreased its strength.

4.4 Classification of Mining Ground Cracks

4.4.1 Temporary and Permanent Cracks

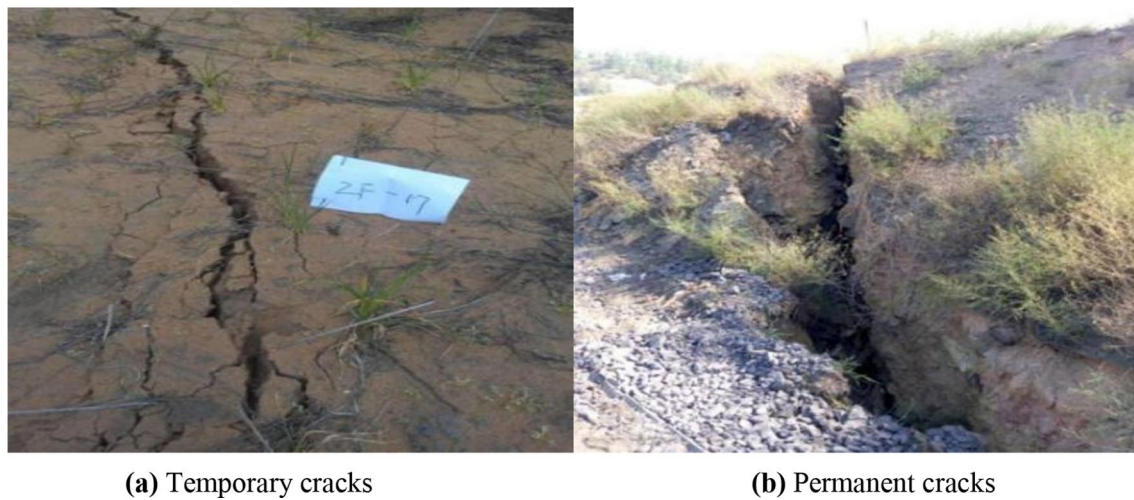
Various ground cracks were formed during lower seam mining. According to the development period, they can be defined as temporary cracks or permanent cracks.

Based on daily observation, temporary cracks were usually produced during the process of the advancement of the working face, as shown in Fig. 13a. Such cracks were mainly formed in the middle part of the working face and caused by the uncoordinated deformation of the ground surface resulting from the breakage of overlying rock strata with the advancement of the working face. However, most of them were closed because of the compression deformation of the ground surface after advancement of the working face. Therefore, the development of such cracks was synchronized with the advancement of the working face. Generally, it is difficult to recognize them after the advancement of the working face because of the rapid change.

Permanent cracks usually occurred at the boundary of the working face, that is, the area where the horizontal deformation is the largest after ground deformation stabilized, as shown in Fig. 13b. From formation to stabilization, which is a slow process, the width and depth gradually increased and became permanent. If a large number of permanent cracks developed, they may well cause soil erosion, degradation of the surface vegetation, and destruction of the ecological environment of the western mining area. In an effort to protect the ecological environment in mining area, such cracks were usually backfilled after recovery.

Table 2 Comparison of relative parameters of surface deformation

Zone	Maximum subsidence (mm)	Advance influence distance (m)	Advance angle of influence (°)	Lagging angle of maximum subsidence velocity (°)	Subsidence coefficient
Overlying previous gob	5847	101.7	44.52	35.54	0.86
Overlying pillar zone	3638	65.33	56.84	48.01	0.53



(a) Temporary cracks

(b) Permanent cracks

Fig. 13 Mining ground cracks classified by developing period. **a** Tensile cracks, **b** compressive cracks

4.4.2 Tensile and Compressive Cracks

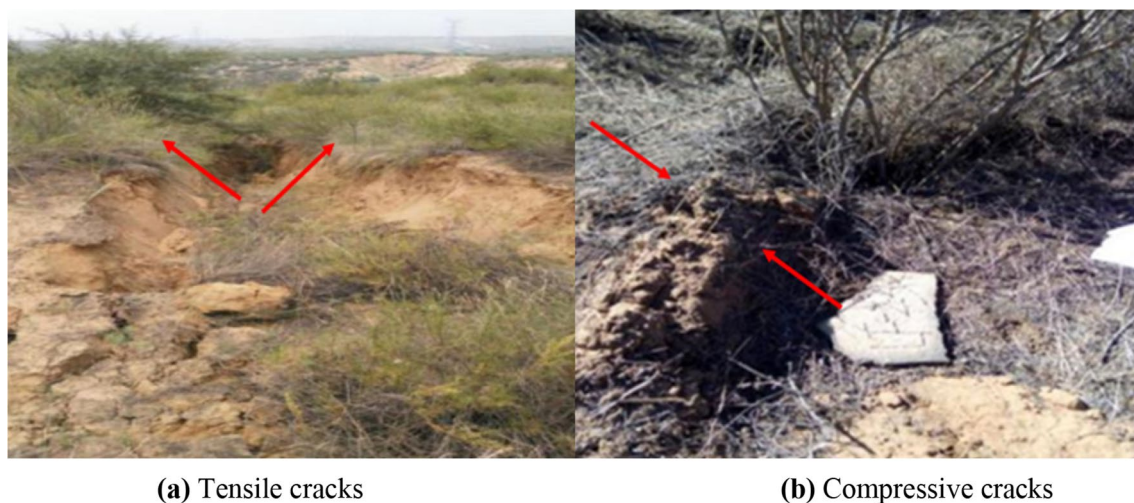
Tensile cracks (Fig. 14a) were caused by the horizontal tensile deformation of the ground surface exceeding the limited tensile strain of the ground surface layer during advancement of the working face. They were mainly distributed in the tensile deformation zone of the ground surface, and generally before or after the working face. Besides, the depth and width of tensile cracks were usually small, and the development process was easily observed despite its rapid variation.

Compressive cracks (Fig. 14b) mainly resulted from the compression deformation exceeding the limited compression strain of the ground surface. They were mainly distributed in the compression deformation zone of the ground surface, and their occurrence usually lagged behind the working face.

4.4.3 Collapsed and Slipped Cracks

The collapsed cracks were caused by the collapse of the ground surface resulting from the overlying strata fracturing due to mining activities. They were mainly located on the ground surface above the working face and developed with the advancement of the working face. Generally, the width and depth were large, as can be seen in Fig. 15a.

The slope slippage and the local breakage of the ground surface because of mining activities easily triggered the slipped cracks, as shown in Fig. 15b. In terms of formation mechanics, they were induced by stretching of the surface due to mining activities combined with the slope slippage, which is different from other types of ground cracks. Cracks were also greatly influenced by the geological and



(a) Tensile cracks

(b) Compressive cracks

Fig. 14 Mining ground fissures classified by developing period. **a** Collapsed cracks, **b** slipped cracks



Fig. 15 Mining ground cracks classified by developing period

geomorphic surroundings. For instance, the topsoil layer was looser when the surface slope was greater, which resulted in cracks readily forming.

4.5 Distribution Characteristics of Ground Cracks

During the observation period, the position, width and depth of ground cracks and their variation with the advancement of the working face 22307 were recorded. Based on the data, combining with the exploitation ichnography, the spatial distribution of ground cracks along the working surface can be obtained, as shown in Fig. 16.

As seen from Fig. 16, the ground cracks were almost located in the middle part of the working face and nearly

perpendicular to the direction of the working face. Obviously, the ground cracks above a previous gob were denser and longer than that above the left pillar. The average interval of the ground cracks above the previous gob was 14.75 m, while that above the pillar zone was 27.8 m. This phenomenon indicates that mining activities caused greater deformation of the ground surface above the previous gob than of the ground surface above the pillar zone. Furthermore, the ground cracks above the previous gob still existed and hardly changed after advancement of the working face; most of the surface cracks above the pillar zone were closed after advancement of the working face, and only a few were observed. This may be related to the mechanical properties of the overlying strata.

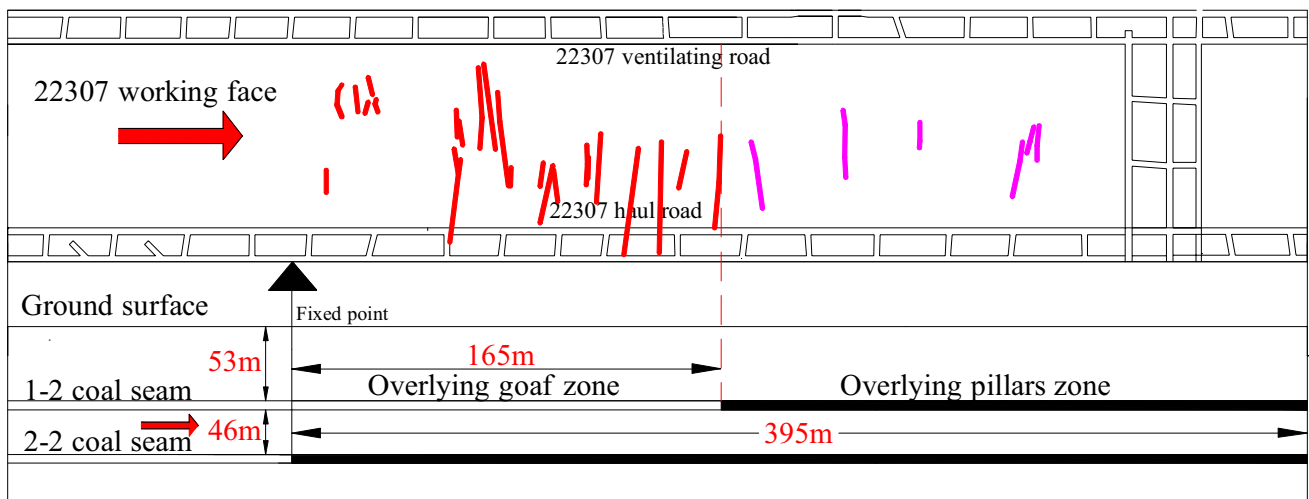


Fig. 16 Ground cracks: partial distribution of 22307 working face

4.6 Development Law of Ground Cracks

Generally, with the influence of the movement of overlying strata, the ground cracks induced by mining activities would experience formation, expansion, decrescence, and closure. Figure 17 shows the dynamic variation process of the development of typical ground crack CLF1 with the advancement of the working face. At the beginning of the advancement of the working face, the ground crack formed and its width was very small, which resulted in a slight

deformation of the road (Fig. 17a). Then the width of the ground crack gradually increased with the advancement of the working face. Ultimately, the crack width and deformation reached the maximum when the working face exceeded the crack position 6 m (Fig. 17d). Since the expansion of the crack has seriously affected road transportation, workers made a timely backfilling, which prevented continued data collection from the crack. The ground crack variation was strongly associated with the advance rate of the working face. Table 3 lists the variation of relative parameters of the



Fig. 17 Crack CLF1 variation process. **a** August 10th, **b** August 11th, **c** August 12th, **d** August 13th

Table 3 Crack CLF1 change process table

Date	Width (mm)	Length (m)	Step height (mm)	Distance from the working face (m)
August 10	50	10	0	35 m ahead of working face
August 11	180	21	100	23 m ahead of working face
August 12	320	37	300	9 m ahead of working face
August 13	560	55	420	– 6 m ahead of working face

crack CLF1 with the advancement of the working face. A 50-mm-wide ground crack formed 35 m ahead of the working face. With the advancement of the working face, the crack width increased from 50 mm to 560 mm; the length of the crack increased from 10 mm to 55 mm; and the step height increased from 0 mm to 420 mm.

CISMP software (Peng 2009) was employed to predict the horizontal deformation of CLF1 with the advancement of the working face. As can be seen from Fig. 18, at the beginning, the horizontal deformation increased with the increase of crack width. When the working face exceeded the crack position of 6 m, both of them reached the maximum with the width of 560 mm and the horizontal deformation of 4.88 mm/m. However, the horizontal deformation gradually decreased with the advancement of the working face because of surface compression associated with mining activities. When the working face exceeded the crack position of 52 m, the horizontal deformation reached the minimum of 0.07 mm/m. While the specific value of the crack width was unobtainable because of backfilling, based on the later observation data, the crack width did decrease after it reached the maximum.

5 Discussion

5.1 The Evolution Law of Ground Subsidence Induced by Shallow-Buried Close-Distance Multi-seam Mining

The gob is formed after the upper seam extraction, and the initial stress of overlying strata is disturbed and redistributed, thus movement, deformation and destruction of the overlying strata would occur. With the expansion of the gob,

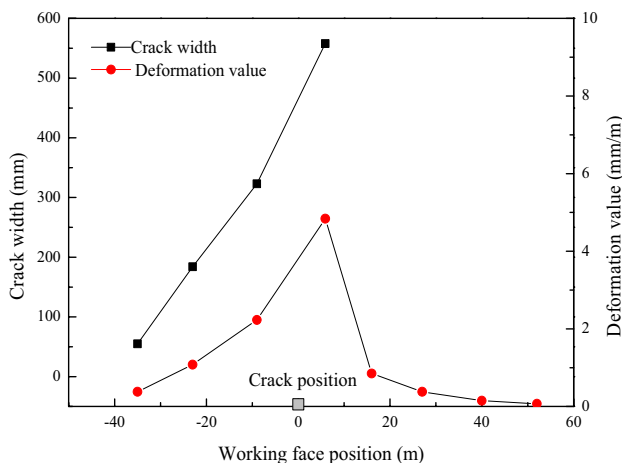


Fig. 18 The relationship between width and horizontal deformation of Fissure CLF1

there was an expansion of the range of rock strata movement. When the gob expanded, the movement of the rock strata spread to the surface, and caused ground surface movement and deformation. Therefore, ground subsidence is the result of the gradual development of overlying strata movement from the bottom to the ground surface after the mining activities.

According to the field measurement in Bulianta Colliery, the ground subsidence (5847 mm) above the previous gob was greater than that above the left pillar (3638 mm). Moreover, the final profile of the ground subsidence basin above the previous gob was steeper than that above the left pillar. The scope of ground surface deformation caused by mining activities above the previous gob is greater than that above the left pillar.

Based on the mining conditions in Bulianta Colliery, the above phenomena can be explained through the following mechanisms:

1. Lower seam mining activated the previous gob. The rock strata immediately overlying on the 2-1 coal seam was broken because of the previous mining activities, then, after a period, the broken rock strata would fall, sink, and accumulate in a loose state in the gob. Although the rock mass has been compacted naturally for a long time, the underground cavity, separation, fracture and pore would still exist for a long time. During repeated mining, the stress equilibrium would be broken again, which again resulted in instability and compaction of the rock mass in the previous gob. Thus, it may induce ground subsidence above the previous gob.
2. As we know, the lithology of overlying rock has significant influence on the dynamic process of ground subsidence and the characteristics of the subsidence basin. The practice shows that the key strata (Pu and Zhang 2011; Coggan et al. 2012) play a major role in controlling movement of overlying strata on the stope. According to the geological data, there were only about 30 m of medium-hard rock strata (Table 2), between the 2-1 coal seam and the 2-2 coal seam, controlling the overlying strata movement; therefore, the bearing capacity of key strata was low. Meanwhile, the previous gob would be activated because of the 2-2 coal seam mining operations, which made the compacted rock loose in the previous gob. Together with the effect of the deadweight of the loose rock, the ground subsidence above the previous gob would be intensified. Compared with the rock in the overlying gob zone, the overlying strata in the left pillar zone were relatively complete and had a large bearing capacity. Therefore, the ground subsidence on the left pillar was smaller than that above the previous gob.
3. In addition, the working panel was covered with 8–23 m of Aeolian sand. Compared with the bedrock, the Aeolian sand has a low bearing capacity, which would lead to ground subsidence.

lian sand had low density, low strength, and no tensile strength, which made it easily deformed when subjected to an external force. Therefore, it did not have the bearing capacity similar to the “beam” structure. Under its own heavy weight, it would produce greater pressure on the lower bedrock. Thus, it sank along with the subsidence of bedrock, but also deformed under the additional stress from mining activities.

5.2 The Formation Mechanism of Ground Cracks Induced by Multi-seam Mining

Based on elastic finite element method analysis, the ground stress distribution in the overburden layer after the extraction is illustrated in Fig. 19. In the figure, (1) is the compressive stress area; (2a) is the tensile stress area; (2b) is the tensile stress area of positive curvature; (3a) is the compressive stress area of negative curvature; and (3b) is the supporting pressure area. The ground surface above the gob (e.g., the underground slope) was located in the horizontally compressive stress scope. Therefore, the compressive cracks would be mostly formed in this area because of the effect of compressive stress. However, previous tensile cracks would be closed because of the effect of compressive stress. Meanwhile, the ground surface above the both sides of the gob was located in the tensile stress area, which resulted in the formation of tensile cracks.

As can be seen from Fig. 19, within the scope of the influence of the mining subsidence, there are both compressive deformation and tensile deformation zone simultaneously on the ground surface. Generally, during the underground mining process, tensile cracks usually occur ahead of the working face, develop in the tensile deformation zone; while compressive cracks occur behind the working face, and develop in the compressive deformation zone on the ground surface.

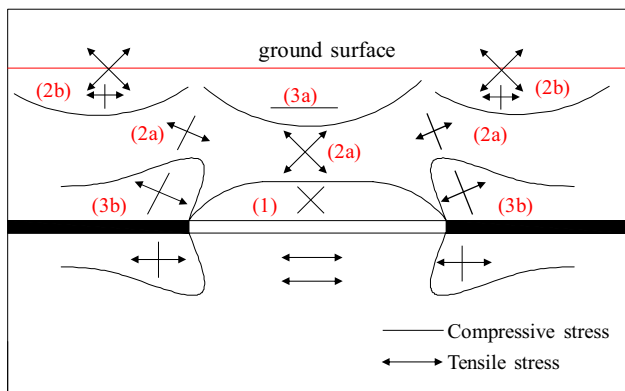


Fig. 19 Stress distribution in the overburden layer after the extraction (Sui 1999)

During the observation period, when the 22307 working face reached 37.25 m from the left side of the border (between overlying goaf zone and overlying pillars zone), a tensile crack C1 was formed at the border; while the working surface advanced to 25 m from the left side of the border, a compressive crack C2 was formed lagging behind 25 m from the crack C1 (Fig. 20). With the continuous advancement of the working face, the surface near the cracks gradually subsided and evolved to a graben. When the working face advanced to 15.65 m from the left side of the border, the subsidence height of the graben was about 100 mm. However, when the working face advanced from 8.4 to 3.2 m from the left side of the border, a strong roof weighting phenomenon occurred and lasted 24 h, which resulted in that the subsidence height of the graben increased from 100 to 900 mm. During this period, the support resistance was in a high level about 18 000 N, which may result from the breakage of the immediate roof.

Therefore, it can be concluded that the ground cracks were formed ahead of the working face and developed rapidly during the period of the breakage of the immediate roof. Generally, the ground cracks above the overlying goaf zone were formed ahead 16.78 m of the working face, while that above the overlying pillars zone were formed ahead 33.5 m of the working face.

5.3 The Effect of Advance Rate of the Longwall Face on the Formation of Ground Cracks

Related studies have shown that advance rate of the longwall face is closely related to the periodic roof weighting and the breaking law of overlying strata, which may directly

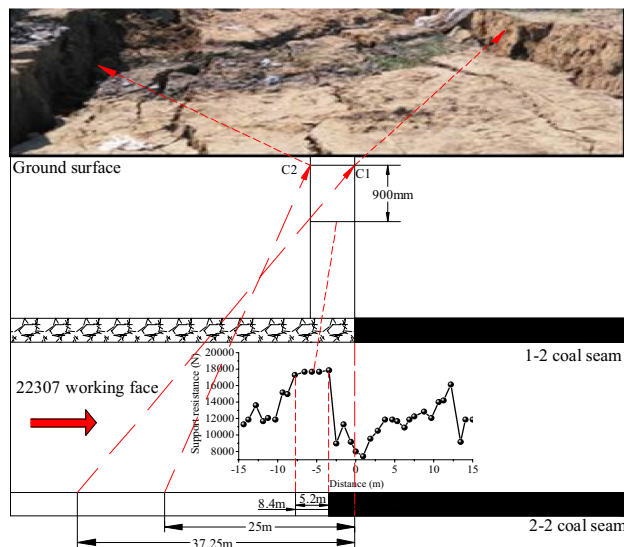


Fig. 20 Development law of surface cracks (modified after Du et al. 2017)

or indirectly influence the ground deformation and the formation and development of ground cracks (Krzysztof et al. 2018; Wang et al. 2018). Generally, with the increase of the advance rate of the working face, the peak distance and the influence range of the abutment pressure show a decreasing trend, as well as the concentration coefficient of in situ stress (Liu 2010), which is conducive to the stability of the overlying strata. However, the loading rate of mining pressure on overlying strata is also affected by the advance rate of the working face, which may intensify the damage of the overlying strata (Yang 2015). Thus, it is necessary to explore the relationship between the formation of ground cracks and the advance rate of the longwall face to guide the field work.

The ground cracks were counted during the advancement of the working face. The advance distance of the tensile cracks was closely related to the advance rate of the working face. The relationship between the advance distance of ground cracks and the advance rate of the working face was fitted in Fig. 21, using a quadratic function. The advance distance of the mining surface crack reached the minimum 13.6 m, when the advance rate of the working face was 12.8 m/day, which indicates that the ground surface was minimally damaged by mining activities.

6 Conclusions

Ground crack and subsidence measurements were conducted after establishing an observation station in the Bulianta Colliery, which has a shallow-buried coal seam and thick, loose layer covering the ground surface. Measurements included the height variation of the observation points, the width variation and positions of ground cracks, the profile and distribution of ground cracks, and

the development of ground cracks with the advancement of the working face.

Through analyzing the data observed from the field, the ground subsidence above the previous (5847 mm) was greater than above the left pillar (3638 mm). The profile of the ground subsidence basin above the previous gob was steeper than that above the left pillar. Mining activities under the previous gob induced more intense deformation and ground subsidence than under the pillar. The advance angle of influence and the lagging angle of maximum subsidence velocity of the ground surface above the previous gob were greater than that above the left pillar, which indicates that the influence scope was greater above the previous gob. Thus, the mechanism of ground subsidence induced by multi-mining has been discussed, mainly including the activation of a previous gob caused by mining activities, the low-bearing capacity of key strata, and the strong self-weight of thick loose layer covering the ground surface.

The ground cracks induced by mining activities were classified and summarized depending on their features as temporary cracks or permanent cracks, tensile cracks or compressive cracks, and collapse cracks or slipped cracks. Furthermore, the distribution of ground cracks above the previous gob varied from that above the left pillar. The average distance of the ground cracks above the previous gob was 14.75 m, while that above the left pillar was 27.8 m. Furthermore, the formation mechanisms of tensile cracks and compressive cracks were determined by analyzing the ground stress distribution in the overburden layer after the extraction. The relationship between the advance distance of ground cracks and advance rate of the working face was fitted with a quadratic function. Through calculation, when the advance rate of the working face was 12.8 m/day, the advance distance of the mining surface crack reached the minimum of 13.6 m. This finding is helpful for protection of the surficial environment during and after mining operations.

In addition to the results presented in this paper, there are a few issues that should be clarified in future work. First, the movement of overlying rock strata directly relates to the deformation of the ground surface. Thus, the different movement mechanisms of overlying strata should be explored and combined with the deformation of the ground surface. Second, although the mechanisms for ground subsidence and crack formation were identified for this site, they may not be applicable for other mining conditions. Therefore, different mining conditions should be considered, such as properties of the rock strata, mining depth, and mining methods, to improve and perfect the above mechanisms. Third, corresponding protection operations for the ground surface should be developed for the mechanisms, so that they are systematic and standardized for different mining conditions.

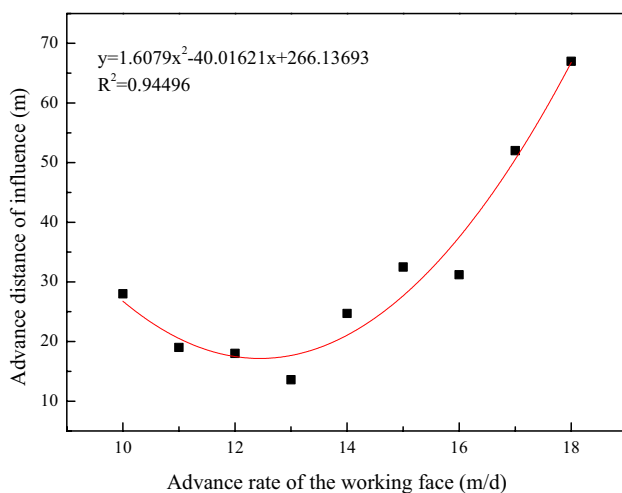


Fig. 21 Advance distance of ground cracks and advance rate simulation relation

Acknowledgements This study was financially supported by project (51574280, 51774319, 51874348)—National Natural Science Foundation of China, project (cstc2015jcyjBX0076)—Basic Science and Frontier Technology Research Project of Chongqing, project (2016ZX05045004)—National Science and Technology Major Project of China. The authors thank Mr. Wang Chen who has conducted a lot of field work, and the authors also thank the editor and anonymous reviewers very much for their valuable advices.

References

- Bian HF, Zhang SB, Zhang QZ, Zheng NS (2014) Monitoring large-area mining subsidence by GNSS based on. *IGS Stn Trans Non-ferrous Metals Soc China* 24(2):514–519
- Can E, Kuşcu Ş, Mekik C (2012) Determination of underground mining induced displacements using GPS observations in Zonguldak-Kozlu hard coal basin. *Int J Coal Geol* 89:62–69
- Can E, Mekik Ç, Kuşcu Ş, Akçın H (2013) Computation of subsidence parameters resulting from layer movements post-operations of underground mining. *J Struct Geol* 47:16–24
- Coggan J, Gao F, Stead D, Elmo D (2012) Numerical modelling of the effects of weak immediate roof lithology on coal mine roadway stability. *Int J Coal Geol* 90–91:100–109
- Deck O, Anirudh H (2010) Numerical study of the soil–structure interaction within mining subsidence areas. *Comput Geosci* 37:802–816
- Ding K, Ma FS, Guo J, Zhao HJ, Lu R, Liu F (2017) Investigation of the Mechanism of Roof Caving in the Jinchuan Nickel Mine, China. *Rock Mech Rock Eng* 51:1215–1226
- Do TN, Wu J, Lin H (2017) Investigation of sloped surface subsidence during inclined seam extraction in a jointed rock mass using discontinuous deformation analysis. *Int J Geomech* 17(8):04017021
- Du F, Yuan RF, Zheng JL, Song GJ (2017) Mechanism of abnormal strata pressure of mining under coal pillar in close distance shallow coal seams. *J China Coal Soc* 42(S1):24–29
- Falcón S, Gavete L, Ruiz A (1996) A model to simulate the mining subsidence problem coding and implementation of the algorithm. *Comput Geosci* 22:897–906
- Fan GW, Zhou L (2010) Mining-induced variation in water levels in unconsolidated aquifers and mechanisms of water preservation in mines. *Min Sci Technol* 20:0814–0819
- Feng JJ, Wang EY, Chen X (2018) Energy dissipation rate: an indicator of coal deformation and failure under static and dynamic compressive loads. *Int J Min Sci Technol* 28(3):397–406
- Ghabraie B, Ren G, Zhang XY, Smith J (2015) Physical modeling of subsidence from sequential extraction of partially overlapping longwall panels and study of substrata movement characteristics. *Int J Coal Geol* 140:71–83
- Ghabraie B, Ren G, Smith JV (2017) Characterising the multi-seam subsidence due to varying mining configuration, insights from physical modeling. *Int J Rock Mech Min Sci* 93:269–279
- Ghosh G, Sivakumar C (2018) Application of underground microseismic monitoring for ground failure and secure longwall coal mining operation: a case study in an Indian mine. *J Appl Geophys* 150:21–39
- Guo K, Wu S, Xu Y (2017a) Face recognition using both visible light image and nearinfrared image and a deep network. *CAAI Trans Intell Technol* 2(1):39–47
- Guo WB, Bai E, Yang DM (2017b) Surface subsidence characteristics and damage protection techniques of high-intensity mining in China. *Adv Coal Mine Ground Control* 6:157–203
- Hamdi P, Stead D, Elmo D, Töyrä J (2018) Use of an integrated finite/discrete element method-discrete fracture network approach to characterize surface subsidence associated with sublevel caving. *Int J Rock Mech Min Sci* 103:55–67
- Holla L, Buizen M (1991) The ground movement, strata fracturing and changes in permeability due to deep longwall mining. *Int J Rock Mech Min Sci Geomech Abstr* 28:207–217
- Hu ZQ, Wang XJ, He AM (2014) Distribution characteristic and development rules of ground fissures due to coal mining in windy and sandy region. *J China Coal Soc* 39(1):11–18
- Hu ZX, Hu XM, Cheng WM, Zhao YY, Wu MY (2018) Performance optimization of one-component polyurethane healing agent for self-healing concrete. *Constr Build Mater* 179:151–159
- Hyun JO, Saro L (2011) Integration of ground subsidence hazard maps of abandoned coal mines in Samcheok, Korea. *Int J Coal Geol* 86:58–72
- Ju J, Xu J (2015) Surface stepped subsidence related to top-coal caving long wall mining of extremely thick coal seam under shallow cover. *Int J Rock Mech Mining Sci* 78:27–35
- Krzysztof T, Rafał M, Anton S (2018) Analysis of the surface horizontal displacement changes due to longwall panel advance. *Int J Rock Mech Min Sci* 104:119–125
- Li WX, Dai LF, Hou XB, Lei W (2007) Fuzzy genetic programming method for analysis of ground movements due to underground mining. *Int J Rock Mech Min Sci* 44:954–961
- Li WX, Wen L, Liu XM (2010) Ground movements caused by deep underground mining in Guan-Zhuang Iron Mine, Luzhong, China. *Int J Appl Earth Obs Geoinf* 12(3):175–182
- Li XL, Wang EY, Li ZH (2016) Rock burst monitoring by integrated microseismic and electromagnetic radiation methods. *Rock Mech Rock Eng* 49(11):4393–4406
- Li XL, Li ZH, Wang EY (2018) Pattern recognition of mine microseismic (MS) and blasting events based on wave fractal features. *Fractals*. 26(3):1850029–1–1850029–18
- Liu QM (2010) Analysis on mining velocity effect of mine pressure behavior of fully mechanized longwall coal mining face with shallow mining depth. *Coal Sci Technol* 38(7):24–26
- Liu QM, Li WP, Li XQ, Hu G (2011) Study on deformation characteristics of coal roof overlapping mining under the coverage of magmatic rocks with DEM simulation. *Pro Eng* 26:101–106
- Lu SQ, Li L, Cheng YP (2017) Mechanical failure mechanisms and forms of normal and deformed coal combination containing gas: model development and analysis. *Eng Fail Anal* 80:241–252
- Manekar G, Shome D, Chaudhari M (2017) Prediction of subsidence parameters & 3-D analysis at Balaghat underground manganese mine of MOIL limited. *India Pro Eng* 191:1075–1086
- Mckee DW, Clement SJ, Almutairi J (2018) Survey of advances and challenges in intelligent autonomy for distributed cyber-physical systems. *CAAI Trans Intell Technol* 3(2):75–82
- Newman C, Agioutantis Z, Leon GB (2017) Assessment of potential impacts to surface and subsurface water bodies due to longwall mining. *Int J Min Sci Technol* 27:57–64
- Park I, Choi J, Lee MJ (2012) Application of an adaptive neuro-fuzzy inference system to ground subsidence hazard mapping. *Comput Geosci* 48:228–238
- Peng SS (2009) CISP—comprehensive and integrated subsidence prediction model USER'S MANUAL. Department of Mining Engineering, College of Engineering and Mineral Resources, West Virginia University, Morgantown
- Pu H, Zhang J (2011) Mechanical model of control of key strata in deep mining. *Min Sci Technol* 21:267–272
- Qian C, Fang YC (2018) Adaptive tracking control of flapping wing micro-air vehicles with averaging theory. *CAAI Trans Intell Technol* 3(1):18–27
- Ren G, Li G, Kulassa M (2014) Application of a generalized influence function method for subsidence prediction in multi-seam longwall extraction. *Geotech Geol Eng* 32(4):1123–1131

- Salmi EF, Nazem M, Karakus M (2017) Numerical analysis of a large landslide induced by coal mining subsidence. *Eng Geol* 217:141–152
- Sasaoka T, Takamoto H, Shimada H, Oya J, Hamanaka A, Matsui K (2015) Surface subsidence due to underground mining operation under weak geological condition in Indonesia. *J Rock Mech Geotech Eng* 7:337–344
- Sepehri M, Apel DB, Hall RA (2017) Prediction of mining-induced surface subsidence and ground movements at a Canadian diamond mine using an Elastoplastic finite element model. *Int J Rock Mech Min Sci* 100:73–82
- Shabanimashcool M, Li CC (2012) Numerical modelling of longwall mining and stability analysis of the gates in a coal mine. *Int J Rock Mech Min Sci* 51:24–34
- Shahab DM (2011) Reservoir simulation and modeling based on artificial intelligence and data mining (AI&DM). *J Nat Gas Sci Eng* 3:697–705
- Shen WL, Bai JB, Li WF, Wang XY (2018) Prediction of relative displacement for entry roof with weak plane under the effect of mining abutment stress. *Tunn Undergr Space Technol* 71:309–317
- Singh G (2015) Conventional approaches for assessment of caving behavior and support requirement with regard to strata control experiences in longwall workings. *J Rock Mech Geotech Eng* 7:291–297
- Suchowerska A, Merifield R, Carter J (2013) Vertical stress changes in multi seam mining under supercritical longwall panels. *Int J Rock Mech Min Sci* 61:306–320
- Suchowerska A, Carter J, Hambleton J (2016) Geomechanics of subsidence above single and multi-seam coal mining. *J Rock Mech Geotech Eng* 8:304–313
- Sui W (1999) Engineering geological study on soil mass deformation during subsidence. Monograph. China University of Mining & Technology, Xuzhou
- Torres JJ, Rodriguez CA (2017) Metaheuristic post-optimization of the NIST repository of covering arrays. *CAAI Trans Intell Technol* 2(1):31–38
- Tzampoglou P, Loupasakis C (2018) Evaluating geological and geotechnical data for the study of land subsidence phenomena at the perimeter of the Amyntaio coalmine, Greece. *Int J Min Sci Technol* 28:601–612 (in press)
- Wang GF, Zhang DS (2018) Innovation practice and development prospect of intelligent fully mechanized technology for coal mining. *J China Univ Min Technol* 47:459–467
- Wang SF, Li XB, Wang SY (2017) Separation and fracturing in overlying strata disturbed by longwall mining in a mineral deposit seam. *Eng Geol* 226:257–266
- Wang CL, Zhang CS, Zhao XD, Liao L, Zhang SL (2018) Dynamic structural evolution of overlying strata during shallow coal seam longwall mining. *Int J Rock Mech Min Sci* 103:20–32
- Wu K, Li L, Wang XL, Zhang LG, Wang ZS, Sun XM (2009) Research of ground cracks caused by fully mechanized sublevel caving mining based on field survey. 6th Int Conf Min Sci Technol Proc Earth Planet Sci 1:1095–1100
- Wu SC, Han LQ, Li ZP, Guo C, Zhou JX (2018) Discussion on the methods for determining slope safety factor based on stress state of the sliding surface. *J China Univ Min Technol* 47:719–726
- Xia KZ, Chen CX, Fu H, Pan YC, Deng YY (2016) Mining-induced ground deformation in tectonic stress metal mines: a case study. *Eng Geol* 210:212–230
- Xie JL, Xu JL, Wang F, Guo JK, Liu DL (2014) Deformation effect of lateral roof roadway in close coal seams after repeated mining. *Int J Min Sci Technol* 24(5):597–601
- Xu YX (2015) Coal mining science (monograph). China University of Mining and Technology, Xuzhou
- Xuan DY, Xu JL, Wang BL, Hong T (2015) Borehole Investigation of the effectiveness of grout injection technology on coal mine subsidence control. *Rock Mech Rock Eng* 48:2435–2445
- Yang JH (2015) Effect of displacement loading rate on mechanical properties of sandstone. *Electron J Geotech Eng* 20(02):591–602
- Zhang Z, Nemcik J (2013) Friction factor of water flow through rough rock fractures. *Rock Mech Rock Eng* 46(5):1125–1134
- Zhang X, Hu XM, Wu MY, Zhao YY, Yu C (2018) Effects of different catalysts on the structure and properties of polyurethane/water glass grouting materials. *J Appl Polym Sci* 135:27
- Zhao T, Zhang Z, Tan Y, Shi C, Wei P, Li Q (2014) An innovative approach to thin coal seam mining of complex geological conditions by pressure regulation. *Int J Rock Mech Min Sci* 71:249–257
- Zhou DW, Wu K, Bai ZH, Hu ZQ, Li L, Xu YK, Xinpeng D (2017) Formation and development mechanism of ground crack caused by coal mining: effects of overlying key strata. *Bull Eng Geol Environ* 76:1–20
- Zhu WB (2010) Study on the instability mechanism of key strata structure in repeated mining of shallow close distance seams. Ph.D. Dissertation. University of Mining and Technology, China
- Zhu GH, Lian DJ (2012) Analysis on mining induced cumulative effective of surface cracks in mining areas. *J Saf Sci Technol* 8(5):47–52
- Zhu D, Tu S (2017) Mechanisms of support failure induced by repeated mining under gobs created by two-seam room mining and prevention measures. *Eng Fail Anal* 82:161–178
- Zou QL, Lin BQ (2017) Modeling the relationship between macro- and meso-parameters of coal using a combined optimization method. *Environ Earth Sci* 76(14):479
- Zou QL, Lin BQ (2018) Fluid-solid coupling characteristics of gas-bearing coal subject to hydraulic slotting: an experimental investigation. *Energy Fuels* 32(2):1047–1060
- Zuo JP, Peng SP, Li YJ, Chen ZH, Xie HP (2009) Investigation of karst collapse based on 3 D seismic technique and DDA method at Xieqiao coal mine, China. *Int J Coal Geol* 78:276–287

Publisher's Note Springer Nature remains neutral with regard to jurisdictional claims in published maps and institutional affiliations.